

# Terahertz Spectra Revealing the Collective Excitation Mode in Charge-Density-Wave Single Crystal $\text{LuFe}_2\text{O}_4$

Xiumei Liu, Zuanming Jin,\* Zhenxiang Cheng,\* Xian Lin, Geetha Balakrishnan, and Guohong Ma\*

A low-energy collective excitation mode in charge-ordered multiferroic  $\text{LuFe}_2\text{O}_4$  is reported via terahertz time-domain spectroscopy. Upon cooling from 300 to 40 K, the central resonance frequency showed a pronounced hardening from 0.85 to 1.15 THz. In analogy to the well-known low-energy optical properties of  $\text{LuFe}_2\text{O}_4$ , this emerging resonance was attributed to the charge-density-wave (CDW) collective excitations. By using the Drude-Lorentz model fitting, the CDW collective mode becomes increasingly damped with the increasing temperature. Furthermore, the kinks of the CDW collective mode at the magnetic transition temperature are analyzed, which indicate the coupling of spin order with electric polarization.

The multiferroics are materials that exhibit both ferroelectricity and magnetic order in a common range of temperature.<sup>[1,2]</sup> The multiferroics are widely used in modern electronics, such as memory elements, filtering devices, and high-performance insulators.<sup>[3]</sup> Mixed valence material  $\text{LuFe}_2\text{O}_4$  is one of the novel multiferroics, which originates from peculiar polarization mechanism compared with the typical ferroelectrics.<sup>[4,5]</sup> Raman,<sup>[6,7]</sup> infrared (IR),<sup>[8]</sup> and neutron diffraction spectroscopy<sup>[9]</sup> investigations have been carried out on  $\text{LuFe}_2\text{O}_4$ , illustrating its structural, charge ordering, and ferrimagnetic order properties. Initial studies revealed bulk ferroelectric order below the charge ordering temperature,  $T_{\text{CO}} \sim 320$  K, resulting in a spontaneous electric polarization, that further increased upon the appearance of ferrimagnetic spin order below  $T_{\text{N}} \sim 240$  K. In addition, a magneto-structural, first-order type transition has been observed at  $T_{\text{LT}} = 175$  K, which is dependent on the precise oxygen content of the samples.<sup>[10]</sup>

Because the formation of charge ordering between Fe atom-layers breaks the inversion symmetry,  $\text{LuFe}_2\text{O}_4$  composed of the

layer structure with triangle lattice including Fe ions.<sup>[11,12]</sup> Actually, charge order can be described in terms of charge-density-waves (CDW), Yamada et al. showed that the  $\text{LuFe}_2\text{O}_4$  system stabilized in the lowest temperature is characterized by an incommensurate CDW state.<sup>[13,14]</sup> Additionally, in situ cooling transmission electron microscopy shows that the charges at low temperatures are crystallized in a charge-stripe phase, in which the CDW behavior in a nonsinusoidal fashion results in elemental electric dipoles for ferroelectricity.<sup>[15]</sup> CDW, the modulation in the real space charge distribution, is typically associated with a distortion of the lattice, resulting in new excitations in infrared or Raman spectroscopy.<sup>[16–18]</sup>

On the other hand, spin and charge frustrated multiferroic  $\text{LuFe}_2\text{O}_4$  has attracted much for a decade, owing to the observation of strong magnetoelectric coupling near room temperature.<sup>[19–23]</sup> Although previous Raman and infrared studies have shown lattice anomalies through the successive electronic and magnetic transitions, the intrinsic charge dynamics and its role on the magnetoelastic coupling remains unclear. Recently, Lee et al. used ultrafast optical spectroscopy to show the influence of magnetic ordering on quantum charge fluctuations, which can govern the interplay between electric polarization and magnetism.<sup>[24,25]</sup>

Indeed, the terahertz time-domain spectroscopy (THz TDS) is a powerful tool to study the low frequency properties of dielectric materials,<sup>[26–29]</sup> and the THz spintronics.<sup>[30–35]</sup> Much efforts have been devoted to the intriguing phenomenon of charge ordering in  $\text{La}_{0.25}\text{Ca}_{0.75}\text{MnO}_3$  by THz TDS.<sup>[36,37]</sup>

In this letter, we report the measurements of the equilibrium dielectric characteristics of  $\text{LuFe}_2\text{O}_4$  within THz range. A low-energy collective excitation mode was observed below 300 K, which originates from the CDW of  $\text{LuFe}_2\text{O}_4$ . In addition, its temperature dependence suggests that electric polarization is found to be extremely susceptible to spin ordering. We combine THz TDS with magnetic characterization to gain a deeper understanding of magnetoelectric coupling in  $\text{LuFe}_2\text{O}_4$  single crystal.

A single crystal platelet with the *c*-axis perpendicular to the *ab* plane was obtained from a  $\text{LuFe}_2\text{O}_4$  single crystal.<sup>[9]</sup> The crystal growth was performed with optical floating-zone furnaces (Crystal Systems, Inc.) in a flowing  $\text{CO}/\text{CO}_2$  atmosphere (ratio 17/83%). Feed and seed rods counter-rotated in this setup at 30 rpm, with the growth proceeding at  $0.5\text{--}1$  mm  $\text{h}^{-1}$ . The initial growth was performed with polycrystalline seed rods, but

X. Liu, Dr. Z. Jin, X. Lin, Prof. G. Ma  
Department of Physics  
Shanghai University, 99 Shangda Road, Shanghai  
200444, P. R. China  
E-mail: physics\_jzm@shu.edu.cn; ghma@staff.  
shu.edu.cn

Prof. Z. Cheng  
Institute for Superconducting and Electronic  
Materials  
University of Wollongong, New South Wales  
2500, Australia cheng@uow.edu.au

Prof. G. Balakrishnan  
Department of Physics  
University of Warwick, Coventry CV4 7AL, UK

DOI: 10.1002/pssr.201700177

subsequent growths used a cleaved single crystal as a seed. The growths of LuFe<sub>2</sub>O<sub>4</sub> typically yielded multigrain samples. The high-quality single-grain crystals used here were cleaved from such growth sample. The sample was polished on both sides and has a thickness of 0.72 mm. LuFe<sub>2</sub>O<sub>4</sub> belongs to the rhombohedral system (*R*-3m) and consists of two typical layers stacked alternately along the *c*-axis direction, the hexagonal double layers of Fe ions are sandwiched by Lu<sub>2</sub>O<sub>3</sub> layers, which is depicted in Figure 1(a).

Figure 1(b) shows the temperature-dependent zero-field-cooled (ZFC) and field cool warming (FCW) magnetization data of the LuFe<sub>2</sub>O<sub>4</sub> single crystal sample measured at an applied field of 0.01 T. Two magnetic transitions can be observed from the data. A peak at ~240 K, which is attributed to the ferrimagnetic ordering of spins of charge-ordered Fe<sup>2+</sup> and Fe<sup>3+</sup> ions. While a second transition is observed at  $T_{LT} \approx 175$  K, which is reported to be associated with the changes in the magnetic structure with antiferromagnetic nature.<sup>[10]</sup> Our data agree with what was reported for single crystal LuFe<sub>2</sub>O<sub>4</sub>.<sup>[38]</sup>

The normal-incidence THz transmission of the LuFe<sub>2</sub>O<sub>4</sub> was measured with a standard low-temperature-grown (LT) GaAs-based terahertz time-domain spectroscopy (THz TDS). Briefly, the output of a mode-locked Ti:sapphire laser, with pulse duration of 100 fs, centered wavelength of 800 nm, and repetition rate of 80 MHz (Mai Tai HP-1020, Spectra-Physics), was used to generate and detect the THz transient. The emitter and detector of the THz wave were dipole type LT GaAs photoconductive antennas. The THz beam has a diameter of about 5 mm on the sample. The temperature is varied between 40 and 300 K by using a helium cryostat.

Figure 2 shows the THz transmission spectra with the electric field of THz waves, measured in the temperature range of 40–300 K. The polarization of the THz pulse lies within the *ab*-plane and is perpendicular to the *c*-axis of the sample ( $E_{THz} \perp c$ ). The transmitted electric field of THz pulse through the sample ( $E_{sam}$ ) and the reference ( $E_{ref}$ ) are recorded in time domain, as shown in Figure 2(a). The amplitude of the transmitted terahertz waveforms is reduced due to the absorption of the sample. Figure 2(b) shows the corresponding transmittance spectra obtained by numerical Fourier transformation. With increasing

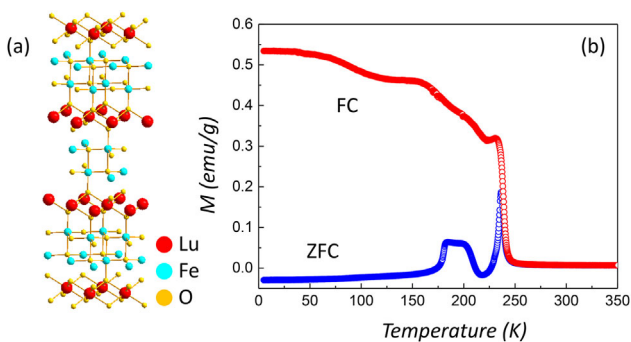


**Figure 1.** (a) The crystal structure of LuFe<sub>2</sub>O<sub>4</sub>. The average valence of Fe ions is Fe<sup>2.5+</sup>, with Fe<sup>2+</sup> and Fe<sup>3+</sup> ions occupying equivalent sites in different layers with equal densities. (b) Susceptibility of the sample measured with a magnetic field of  $H = 100$  Oe applied parallel to the *c*-axis. The blue (red) points denote the ZFC (FC) data.

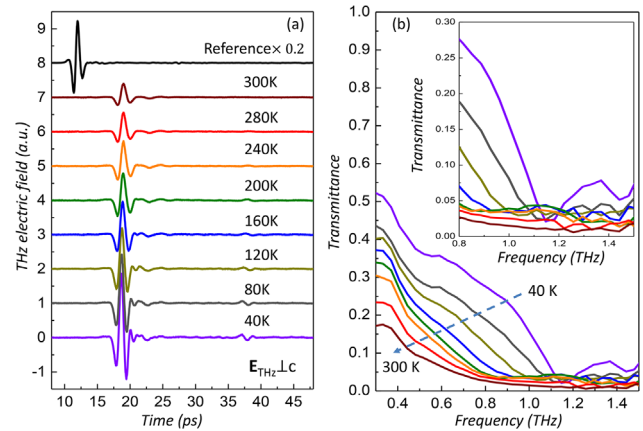


**Figure 2.** (a) Typical THz wave forms in the time-domain of LuFe<sub>2</sub>O<sub>4</sub> measured by electro-optic sampling from 40–300 K in zero magnetic field. (b) The corresponding power transmittance spectrum  $T = E_{sam}(\omega)/E_{ref}(\omega)$  of LuFe<sub>2</sub>O<sub>4</sub> single crystal.

temperature, the transmittance is gradually suppressed, as shown by the arrow. In particular, in the inset of Figure 2(b), a clear absorption peak at around 1.15 THz is observed at 40 K.

With the THz TDS data, we can evaluate the complex refractive index  $\tilde{n}$  without using Kramers–Kronig analysis. The complex spectrum of the transmitted pulse  $E_{sam}(\omega)$  is determined by the product of the input spectrum  $E_{ref}(\omega)$  and the total transmission function of the sample<sup>[39,40]</sup>:

$$\frac{E_{sam}(\omega)}{E_{ref}(\omega)} = t_{12}t_{21}\exp\left(-i\frac{\omega}{c}d(\tilde{n} - 1)\right), \quad (1)$$

where  $t_{12}$  and  $t_{21}$  are the frequency-dependent complex Fresnel transmission coefficients,  $d$  is the thickness of the sample.  $\tilde{n} = n + i\kappa$  is the complex refractive index of the sample. The frequency dependent refractive index  $n$  and power absorption  $\alpha = (4\pi/\lambda)\kappa$  can then be determined by the experimental data directly.

Figure 3(a) shows the power absorption within the frequency region from 0.2 to 1.5 THz. The power absorption gradually increases with increasing frequency. A resonance-like absorption peak appears in the spectra around 0.8 THz below 280 K. Our measurements show that the shape and position of this absorption peak are strongly temperature dependent. A resonance feature clearly appears in the spectra around 1.15 THz at 40 K, which will be discussed later.

Figure 3(b) shows the refractive index at different temperatures. It can be found that the resonant frequency corresponds to the dispersive feature appears in the spectra at 40 K. As shown in the inset of Figure 3(b), the mean value of refractive index over the whole spectral range increases from 3.79 to 3.90 with increasing the temperature from 40 to 300 K.

Upon cooling from room temperature, the charge-ordered phase in LuFe<sub>2</sub>O<sub>4</sub> occurs below  $T_{CO} = 320$  K, followed by ferromagnetic spin order below  $T_N = 240$  K. Therefore, the spin order of the sample should be considered in our LuFe<sub>2</sub>O<sub>4</sub>. We obtain  $[\epsilon\mu]$  spectra via  $\epsilon\mu = \tilde{n}^2$ , where  $\epsilon$  is the complex dielectric constant and  $\mu$  the complex magnetic permeability.

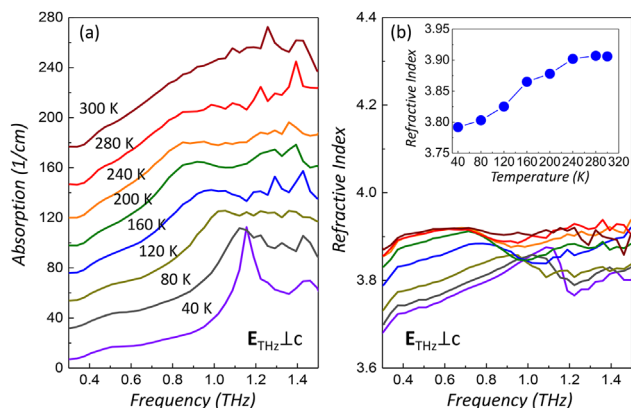


**Figure 3.** (a) Absorption coefficients  $\alpha(\omega)$  and (b) refractive indices  $n(\omega)$  of the *c*-cut  $\text{LuFe}_2\text{O}_4$  crystal. The absorption spectra are offset by  $20\text{ cm}^{-1}$  from each other and labeled with the temperature, from 40 to 300 K. Inset of (b) shows the mean value of the refractive indices within the frequency range of 0.3–1.5 THz, as a function of temperature.

**Figure 4** shows the temperature-dependent real and the imaginary part of the  $[\varepsilon\mu]$  spectra of the  $\text{LuFe}_2\text{O}_4$  single crystal. With decreasing the temperature, both  $\text{Re}[\varepsilon\mu]$  and  $\text{Im}[\varepsilon\mu]$  tend to decrease in magnitude. We can observe the signature of the dispersive structure and resonance peak around 4.6 meV at 40 K in  $\text{Re}[\varepsilon\mu]$  and  $\text{Im}[\varepsilon\mu]$  spectra, respectively. Above 240 K, the broad peak structure is enlarged and obscured, as shown in

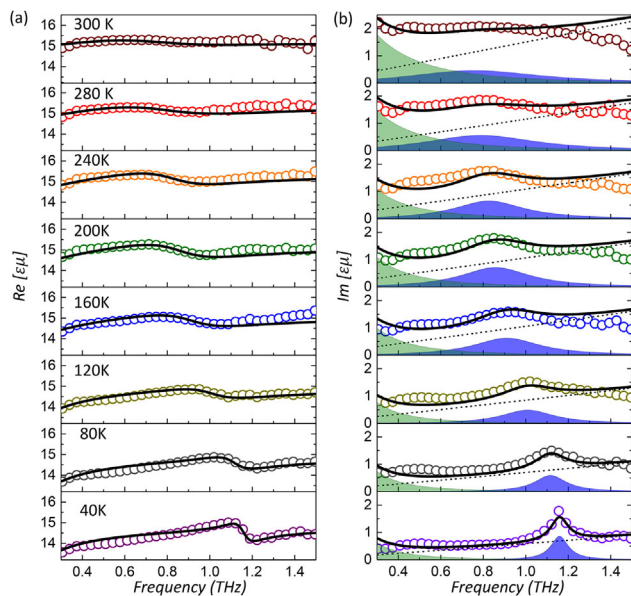


**Figure 4.** Equilibrium optical properties of  $\text{LuFe}_2\text{O}_4$ . (a) Real and (b) imaginary parts of the frequency-dependent equilibrium permittivity  $[\varepsilon\mu]$  at different temperatures. The detection limit in our experiments is 0.15 meV. Circles represent the experimental data. Black lines indicate the fits by Drude–Lorentz model (Eq. (2)). The dashed lines and purple region are components of the background absorption of  $E_u$  mode at around 10 THz (40 meV) and collective excitation mode, respectively. Green region shows the dielectric response based on Drude-term.

$\text{Im}[\varepsilon\mu]$  spectrum. We can not identify the clear signature of the peak structure above 300 K in  $\text{Im}[\varepsilon\mu]$  spectrum.

As previous THz investigation have revealed that the conductivity of  $\text{LuFe}_2\text{O}_4$  does not coincide with the Drude model.<sup>[41,42]</sup> As indicated by the solid lines in Figure 4, we fitted the permittivity spectra using the following Drude–Lorentz (DL) model, to see quantitatively how the observed mode changes with temperature<sup>[43]</sup>:

$$\varepsilon(\omega) = \varepsilon_\infty - \frac{\omega_p^2}{\omega^2 + i\Gamma\omega} + \sum_n \frac{A_n^2}{\omega_n^2 - \omega^2 - i\Gamma_n\omega}, \quad (2)$$

where  $\varepsilon_\infty$  is the relative permittivity as  $\omega$  goes to infinity, the second term is the Drude term with plasma frequency  $\omega_p$  and damping constant  $\Gamma = \frac{1}{\tau}$ . The terms in the summation correspond to the collective excitations with  $A_n$ ,  $\omega_n$ , and  $\Gamma_n$  giving the strength, resonance frequency, and damping of the model, respectively, which hold important information on the charge ordering, will be discussed later.

It is instructive to distinguish the dielectric and magnetic contributions to  $[\varepsilon\mu]$  spectrum, which can be obtained by measuring the THz transmittance and the reflectance spectra simultaneously.<sup>[44,45]</sup> However, we note that a large uncertainty of the measured data at first echo, owing to strong absorption of the crystal. Therefore, in fitting the  $[\varepsilon\mu]$  spectrum, we assumed the magnetic permeability  $\mu \approx 1$ , justified by a much smaller contribution of  $\mu$  to the complex refractive index compared to the  $\varepsilon$ .<sup>[33,46]</sup> It is also noteworthy that the parameters are determined with good accuracy by the fitting on the real and imaginary parts of the dielectric spectrum simultaneously.

As shown in Figure 4(b), we found that the  $\varepsilon(\omega)$  can be well reproduced by a Drude term and two Lorentz terms. Here, we named them as low- and high-frequency mode, respectively. They have different contributions to the  $\varepsilon(\omega)$ : a resonance feature for the low-frequency mode, and a background dispersive feature covering the entire frequency window – the tail of the resonance of high-frequency mode. Note also that the spectral weight of the electronic Drude-term is substantially suppressing as temperature decreased.

Generally, optical absorption of ionic crystals in the far-infrared THz region is attributed to the lattice vibrations.<sup>[28]</sup> The interaction of a radiation field with the fundamental lattice vibration results in absorption of electromagnetic wave due to the creation or annihilation of lattice vibration. We, therefore, assigned the high-frequency mode to the infrared  $E_u$  phonon mode, which corresponds to the motion within the *ab* plane of the  $\text{LuFe}_2\text{O}_4$  single crystal. In the fitting, according to Harris and Yildirim’s symmetry assignments,<sup>[6,47]</sup> we fix the resonant frequency of the high-frequency mode at 10 THz (40 meV) at various temperatures.

We now turn to the low-frequency feature, which was previously assigned to the soft  $\text{TO}_1$  mode.<sup>[41,46]</sup> However, Li et al. could not carry out a detailed study due to low signal-to-noise ratio.<sup>[41]</sup> Usually, the soft phonon mode is closely associated with the symmetry of the crystal before and after the phase transition. A ferroelectric soft phonon  $\text{TO}_1$  mode with the frequency decreasing rapidly at  $T_c$  is the signature of the structure distortion.<sup>[48]</sup> However, the low-frequency mode observed here appears below the lowest optical phonon energy.<sup>[6]</sup> Additionally,

previous studies have shown that the bulk ferroelectric polarization mainly arises from the 3D alternation arrangement of valence-charges, instead of the spatial displacement of cations in the congenital ferroelectric materials.<sup>[4,15,49]</sup>

In order to investigate the origination of the low-frequency resonance, we have explored the temperature dependence from 40 to 300 K. **Figure 5** summarizes the temperature dependence of the resonance frequency  $\omega(T)$  and damping constant  $\Gamma(T)$  of the low-frequency mode in  $\text{LuFe}_2\text{O}_4$ , extracted from the DL fitting. The central frequency  $\omega$  does not considerably change above 240 K, while undergoes a large hardening from 0.85 THz at 240 K to 1.15 THz at 40 K. The resonance frequency not only becomes “hard”, we also find that the spectral shape narrows down. Consequently, the damping constant  $\Gamma$  of the collective excitation mode decreases from 0.8 to 0.1 THz. On the one hand, we note here that the observed structure has a relative small spectral weight compared to the single-particle excitation and spin-density-wave.<sup>[18,50]</sup> On the other hand, herein, the value of  $\Gamma$  is on the same order of that observed in  $\text{Pr}_{0.7}\text{Ca}_{0.3}\text{MnO}_3$ .<sup>[51]</sup> Therefore, qualitatively and quantitatively, our observation of low-frequency collective excitation is in fair agreement with previous experiments reporting the CDW in several manganite systems<sup>[37]</sup> and layered system.<sup>[52,53]</sup>

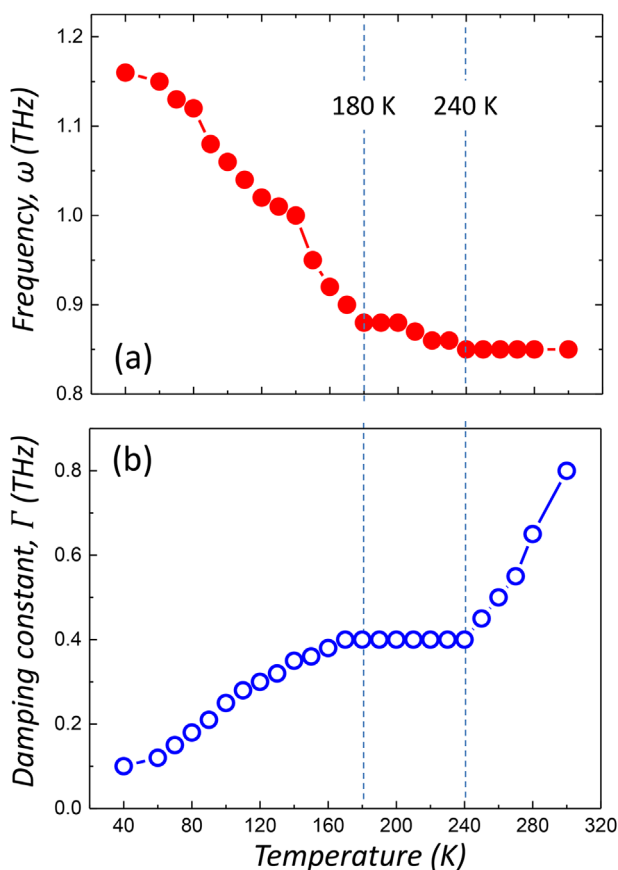


**Figure 5.** Temperature dependences of (a) central frequency and (b) damping constant  $\Gamma$  of the collective amplitude mode. Vertical dashed lines denote the transition temperatures of the magnetic orderings at 180 and 240 K.

We note that the CDW ground state opens band gaps at the Fermi level and exhibits new low-energy collective excitations, the amplitude mode (amplitudon) and phase mode (phason), which correspond to distortions and translations of the modulated charge density.<sup>[54]</sup> Phason is pinned at a finite frequency (usually in the microwave frequency range), due to the presence of impurities or defects. While, the amplitudon involves the ionic displacement and has an energy scale of about 10 meV, even at the  $q=0$  limit.<sup>[53]</sup> Indeed, the assignment of the low-frequency CDW mode to the amplitudon or the phason requires the time and momentum-dependent electronic structures dynamics of  $\text{LuFe}_2\text{O}_4$ . The time- and angle-resolved photoemission spectroscopy (tr-ARPES) is presently beyond the capabilities of our experiments.

Finally, as shown in Figure 5(b),  $\Gamma$  decreases from 0.8 THz (300 K) to 0.4 THz (240 K) significantly and then from 0.4 THz (180 K) to 0.1 THz (40 K), with two clear kinks around  $T_N=240$  K and  $T_{LT}=180$  K. This magnetic ordering tuning effect suggests the magnetoelectric coupling in  $\text{LuFe}_2\text{O}_4$ .

The physics picture observed here can be qualitatively discussed as follows. In general, magnetic ordering can modify the effective hopping amplitude between two Fe ions via the double-exchange mechanism.<sup>[55]</sup> That is, the hopping is governed by the angle between the two core spins. The change in the hopping amplitude will necessarily affect the quantum fluctuations of charge ordered state.<sup>[24]</sup>

We observe that (i) as shown in Figure 2(b), the magnetization increases as the temperature below  $T_N$ ; (ii) as shown in Figure 4(b), the spectral weight of the free carrier Drude-term gradual decreases with decreasing the temperature, indicating the suppressed average hopping amplitude at low temperature. Therefore, by decreasing the charge hopping through the double exchange mechanism, the increased ferromagnetic spin ordering (below 240 K) increases the polarization below  $T_N$ . This is also the reason for hardening of the frequency of the CDW collective mode below 240 K. The observed anomalies on  $\omega(T)$  and  $\Gamma(T)$  are originated from the different spin structure across two magnetic transitions, which indeed deserve further investigation.

In conclusion, we have reported here an investigation of the spin- and charge-ordered multiferroic  $\text{LuFe}_2\text{O}_4$  in the THz range, by using the THz-TDS. The real and imaginary parts of the dielectric constants were accurately determined in the frequency range from 0.2 to 1.5 THz (0.82–6.15 meV). We have found broad resonance shoulder appears below  $T_{CO} \sim 320$  K, and shifts to higher frequency with narrower bandwidth below  $T_N \sim 240$  K, which have been assigned to the CDW collective excitation mode in  $\text{LuFe}_2\text{O}_4$  single crystal. We also discussed the magnetoelectric coupling in  $\text{LuFe}_2\text{O}_4$  by the correspondence between the evolution of the THz CDW collective excitation and the magnetic behavior. We hope that our analysis will gain a deeper understanding of charge ordering in  $\text{LuFe}_2\text{O}_4$  single crystal, which provide the essential information for fundamental properties and potential applications.

## Acknowledgements

This work is supported by the National Natural Science Foundation of China (NSFC, Nos. 11604202, 11674213). Z. J. thanks the Young Eastern

Scholar (QD2015020) at Shanghai Institutions of Higher Learning and the Colleges, Universities Young Teachers Training Funding Program (ZZSD15098) and “Chen Guang” project (16CG45) supported by Shanghai Municipal Education Commission and Shanghai Education Development Foundation. Z. X. Cheng thanks Australia Research Council for financial support. The work at the University of Warwick was supported by the EPSRC, UK, through Grant EP/M028771/1.

## Conflict of Interest

The authors declare no conflict of interest.

## Keywords

charge density wave, multiferroics, time-domain terahertz spectroscopy

Received: June 6, 2017

Revised: July 31, 2017

Published online: August 15, 2017

- [1] D. N. Basov, R. D. Averitt, D. Marel, M. Dressel, K. Haule, *Rev. Mod. Phys.* **2011**, *83*, 471.
- [2] R. Ramesh, N. A. Spaldin, *Nature Mater.* **2007**, *6*, 21.
- [3] S. Fusil, V. Garcia, A. Barthelemy, M. Bibes, *Annu. Rev. Mater. Res.* **2014**, *44*, 91.
- [4] N. Ikeda, T. Nagata, J. Kano, S. Mori, *J. Phys.: Condens. Matter* **2015**, *27*, 053201.
- [5] J. A. Mundy, C. M. Brooks, M. E. Holtz, J. A. Moyer, H. Das, A. F. Rébola, J. T. Heron, J. D. Clark-son, S. M. Disseler, Z. Liu, A. Farhan, R. Held, R. Hovden, E. Padgett, Q. Mao, H. Paik, R. Misra, L. F. Kourkoutis, E. Arenholz, A. Scholl, J. A. Borchers, W. D. Ratcliff, R. Ramesh, C. J. Fennie, P. Schiffer, D. A. Muller, D. G. Schlom, *Nature* **2016**, *537*, 523.
- [6] A. Glamazda, K.-Y. Choi, P. Lemmens, D. Wulferding, S. Park, S.-W. Cheong, *Phys. Rev. B* **2013**, *87*, 144416.
- [7] F. Sun, R. Wang, C. Aku-Leh, H. X. Yang, R. He, J. Zhao, *Sci. Rep.* **2014**, *4*, 6429.
- [8] F. M. Vitucci, A. Nucara, D. Nicoletti, Y. Sun, C. H. Li, J. C. Soret, U. Schade, P. Calvani, *Phys. Rev. B* **2010**, *81*, 195121.
- [9] S. M. Gaw, H. J. Lewtas, D. F. McMorro, J. Kulda, R. A. Ewings, T. G. Perring, R. A. McKinnon, G. Balakrishnan, D. Prabhakaran, A. T. Boothroyd, *Phys. Rev. B* **2015**, *91*, 035103.
- [10] F. Wang, J. Kim, G. D. Gu, Y. Lee, S. Bae, Y.-J. Kim, *J. Appl. Phys.* **2013**, *113*, 063909.
- [11] N. Ikeda, H. Ohsumi, K. Ohwada, K. Ishii, T. Inami, K. Kakurai, Y. Murakami, K. Yoshii, S. Mori, Y. Horibe, H. Kito, *Nature* **2005**, *436*, 1136.
- [12] M. Fiebig, T. Lottermoser, D. Meier, M. Trassin, *Nature Rev. Mater.* **2016**, *1*, 16046.
- [13] Y. Yamada, K. Kitsuda, S. Nohdo, N. Ikeda, *Phys. Rev. B* **2000**, *62*, 12167.
- [14] N. Ikeda, Y. Yamada, S. Nohdo, T. Inami, S. Katano, *Physica B* **1998**, *241*, 820.
- [15] Y. Zhang, H. X. Yang, C. Ma, H. F. Tian, J. Q. Li, *Phys. Rev. Lett.* **2007**, *98*, 247602.
- [16] G. Grüner, *Density Waves in Solids*. Addison-Wesley, Reading, MA **1994**.
- [17] R. Mankowsky, B. Liu, S. Rajasekaran, H. Y. Liu, D. Mou, X. J. Zhou, R. Merlin, M. Först, A. Cavalleri, *Phys. Rev. Lett.* **2017**, *118*, 116402.
- [18] G. Grüner, *Rev. Mod. Phys.* **1988**, *60*, 1129.
- [19] J. Iida, M. Tanaka, Y. Nakagawa, S. Funahashi, N. Kimizuka, S. Takekawa, *J. Phys. Soc. Jpn.* **1993**, *62*, 1723.
- [20] X. S. Xu, J. de Groot, Q.-C. Sun, B. C. Sales, D. Mandrus, M. Angst, A. P. Litvinchuk, J. L. Musfeldt, *Phys. Rev. B* **2010**, *82*, 014304.
- [21] X. S. Xu, M. Angst, T. V. Brinzari, R. P. Hermann, J. L. Musfeldt, A. D. Christianson, D. Mandrus, B. C. Sales, S. McGill, J.-W. Kim, Z. Islam, Charge Order. *Phys. Rev. Lett.* **2008**, *101*, 227602.
- [22] M. Angst, R. P. Hermann, A. D. Christianson, M. D. Lumsden, C. Lee, M.-H. Whangbo, J.-W. Kim, P. J. Ryan, S. E. Nagler, W. Tian, R. Jin, B. C. Sales, D. Mandrus, *Phys. Rev. Lett.* **2008**, *101*, 227601.
- [23] K.-T. Ko, H.-J. Noh, J.-Y. Kim, B.-G. Park, J.-H. Park, A. Tanaka, S. B. Kim, C. L. Zhang, S.-W. Cheong, *Phys. Rev. Lett.* **2009**, *103*, 207202.
- [24] J. Lee, S. A. Trugman, C. D. Batista, C. L. Zhang, D. Talbayev, X. S. Xu, S.-W. Cheong, D. A. Yarotski, A. J. Taylor, R. P. Prasankumar, *Sci. Rep.* **2013**, *3*, 2654.
- [25] J. Lee, S. A. Trugman, C. L. Zhang, D. Talbayev, X. S. Xu, S.-W. Cheong, D. A. Yarotski, A. J. Taylor, R. P. Prasankumar, *Appl. Phys. Lett.* **2015**, *107*, 042906.
- [26] F. Chen, Y. Zhu, S. Liu, Y. Qi, H. Y. Hwang, N. C. Brandt, J. Lu, F. Quirin, H. Enquist, P. Zalden, T. Hu, J. Goodfellow, M.-J. Sher, M. C. Hoffmann, D. Zhu, H. Lemke, J. Glowina, M. Chollet, A. R. Damodaran, J. Park, Z. Cai, I. W. Jung, M. J. Highland, D. A. Walko, J. W. Freeland, P. G. Evans, A. Vailionis, J. Larsson, K. A. Nelson, A. M. Rappe, K. Sokolowski-Tinten, L. W. Martin, H. Wen, A. M. Lindenberg, *Phys. Rev. B* **2016**, *94*, 180104(R).
- [27] E. Constable, R. Ballou, J. Robert, C. Decorse, J.-B. Brubach, P. Roy, E. Lhotel, L. Del-Rey, V. Simonet, S. Petit, S. deBrion, *Phys. Rev. B* **2017**, *95*, 020415(R).
- [28] J. Han, F. Wan, Z. Zhu, W. Zhang, *Appl. Phys. Lett.* **2007**, *90*, 031104.
- [29] I. Katayama, H. Aoki, J. Takeda, H. Shimosato, M. Ashida, R. Kinjo, I. Kawayama, M. Tonouchi, M. Nagai, K. Tanaka, *Phys. Rev. Lett.* **2012**, *108*, 097401.
- [30] S. Baierl, M. Hohenleutner, T. Kampfrath, A. K. Zvezdin, A. V. Kimel, R. Huber, R. V. Mikhaylovskiy, *Nature Photon.* **2016**, *10*, 715.
- [31] R. V. Mikhaylovskiy, T. J. Huisman, R. V. Pisarev, Th. Rasing, A. V. Kimel, *Phys. Rev. Lett.* **2017**, *118*, 017205.
- [32] Z. Jin, A. Tkach, F. Casper, V. Spetter, H. Grimm, A. Thomas, T. Kampfrath, M. Bonn, M. Klau, D. Turchinovich, *Nature Phys.* **2015**, *11*, 761.
- [33] Z. Jin, Z. Mics, G. Ma, Z. Cheng, M. Bonn, D. Turchinovich, *Phys. Rev. B* **2013**, *87*, 094422.
- [34] T. Kampfrath, M. Battiato, P. Maldonado, G. Eilers, J. Nötzold, S. Mährlein, V. Zbarsky, F. Freimuth, Y. Mokrousov, S. Blügel, M. Wolf, I. Radu, P. M. Oppeneer, M. Münzenberg, *Nature Nanotechnol.* **2013**, *8*, 256.
- [35] T. Kampfrath, A. Sell, G. Klatt, A. Pashkin, S. Mährlein, T. Dekorsy, M. Wolf, M. Fiebig, A. Leitenstorfer, R. Huber, *Nature Photon.* **2011**, *5*, 31.
- [36] T. Zhang, E. Zhukova, B. Gorshunov, D. Wu, A. S. Prokhorov, V. I. Torgashev, E. G. Maksimov, M. Dressel, *Phys. Rev. B* **2010**, *81*, 125132.
- [37] A. Nucara, P. Maselli, P. Calvani, R. Sopracase, M. Ortolani, G. Gruener, M. Cestelli Guidi, U. Schade, J. Garcia, *Phys. Rev. Lett.* **2008**, *101*, 066407.
- [38] M. Hervieu, A. Guesdon, J. Bourgeois, E. Elkaïm, M. Poenar, F. Damay, J. Rouquette, A. Maignan, C. Martin, *Nature Mater.* **2014**, *13*, 74.
- [39] R. Ulbricht, E. Hendry, J. Shan, T. Heinz, M. Bonn, *Rev. Mod. Phys.* **2011**, *83*, 543.
- [40] P. Jepsen, D. Cooke, M. Koch, *Laser Photon. Rev.* **2011**, *5*, 124.
- [41] S. Z. Li, S. J. Luo, R. Fu, B. B. Jin, K. F. Wang, J.-M. Liu, J. F. Ding, X. G. Li, *Appl. Phys. A* **2009**, *96*, 893.

- [42] H. Itoh, K. Itoh, K. Anjyo, H. Nakaya, H. Akahama, D. Ohishi, S. Saito, T. Kambe, S. Ishihara, N. Ikeda, S. Iwai, *J. Lumin.* **2013**, 133, 149.
- [43] J. Sun, N. M. Litchinitser, J. Zhou, *ACS Photon.* **2014**, 1, 293.
- [44] H. Němec, F. Kadlec, P. Kužel, L. Duvillaret, J.-L. Coutaz, *Opt. Commun.* **2006**, 260, 175.
- [45] G. Song, J. Jiang, X. Wang, Z. Jin, X. Lin, G. Ma, S. Cao, *J. Appl. Phys.* **2013**, 114, 243104.
- [46] N. Kida, Y. Ikebe, Y. Takahashi, J. P. He, Y. Kaneko, Y. Yamasaki, R. Shimano, T. Arima, N. Nagaosa, Y. Tokura, *Phys. Rev. B* **2008**, 78, 104414.
- [47] A. B. Harris, T. Yildirim, *Phys. Rev. B* **2010**, 81, 134417.
- [48] V. Železný, Eric Cockayne, J. Petzelt, M. F. Limonov, D. E. Usvyat, V. V. Lemanov, A. A. Volkov, *Phys. Rev. B* **2002**, 66, 224303.
- [49] Y. Zhang, H. X. Yang, Y. Q. Guo, C. Ma, H. F. Tian, J. L. Luo, J. Q. Li, *Phys. Rev. B* **2007**, 76, 184105.
- [50] G. Grüner, *Rev. Mod. Phys.* **1994**, 66, 1.
- [51] N. Kida, M. Tonouchi, *Phys. Rev. B* **2002**, 66, 024401.
- [52] R. Y. Chen, B. F. Hu, T. Dong, N. L. Wang, *Phys. Rev. B* **2014**, 89, 075114.
- [53] R. Y. Chen, S. J. Zhang, M. Y. Zhang, T. Dong, N. L. Wang, *Phys. Rev. Lett.* **2017**, 118, 107402.
- [54] H. Y. Liu, I. Gierz, J. C. Petersen, S. Kaiser, A. Simoncig, A. L. Cavalieri, C. Cacho, I. C. E. Turcu, E. Springate, F. Frassetto, L. Poletto, S. S. Dhesi, Z.-A. Xu, T. Cuk, R. Merlin, A. Cavaller, *Phys. Rev. B* **2013**, 88, 045104.
- [55] C. Zener, *Phys. Rev.* **1951**, 82, 403.